ELSEVIER

Biophysical Chemistry 101–102 (2002) 359–373

Biophysical Chemistry

www.elsevier.com/locate/bpc

The dynamic behavior of CheW from *Thermotoga maritima* in solution, as determined by nuclear magnetic resonance: implications for potential protein–protein interaction sites

Ian J. Griswold, Frederick W. Dahlquist*

Institute of Molecular Biology and Department of Chemistry, University of Oregon, Eugene, OR, USA

Received 15 March 2002; received in revised form 25 March 2002; accepted 25 March 2002

Abstract

Measurements of the ^{15}N relaxation parameters have been used to characterize the backbone dynamics of CheW from *Thermotoga maritima*. The dynamic nature of residues that appeared disordered in our recent solution structure of CheW is confirmed by these dynamics measurements. We have interpreted the data in terms of the Lipari and Szabo 'model-free' approach. The derived order parameter, S^2, the $\{^1H\}-^{15}N$ heteronuclear nuclear Overhauser effect (NOE) values, the chemical exchange rate, R_{ex}, and the internal correlation time, τ_e, show that CheW exhibits considerable motional freedom from the picosecond to millisecond time scales. These regions of the protein cluster within the framework of the three-dimensional structure and may indicate possible binding sites for other protein components of the bacterial chemotaxis receptor-signaling complex. The structure of CheW consists of two five-stranded β-barrel domains that pack together with an extensive hydrophobic core between the domains. Regions highlighted by dynamics measurements co-localize to specific regions of the three-dimensional structure of CheW previously implicated in the formation of bacterial chemotaxis receptor signaling complex. The motional properties of domain 2 of CheW suggest that this domain may be able to experience structural rearrangements that allow the exposure of a hydrophobic surface area that could be used as a binding surface for the other members of the receptor complex. Residues within domain 2 have been implicated in binding interactions for two chemotaxis proteins, CheA and the receptor. We further propose that domain 1 interacts with other components of the chemotaxis machinery, such as CheZ, or in the formation of clusters of signaling components.

Keywords: CheW; Chemotaxis; NMR; Dynamics; Relaxation

1. Introduction

Motile bacteria respond to temporal changes in the chemical environment by making either a net movement away from a chemical repellent or toward a chemical attractant (for reviews see [1,2]). In the absence of temporal changes in the chemical environment, *Escherichia coli* cells exhibit a counter-clockwise bias in the rotation of their flagellar motors. This results in predominantly smooth swimming behavior punctuated by a few episodes of reorientation, called 'tumbles', as

*Corresponding author.
E-mail address: fwd@nmr.uoregon.edu (F.W. Dahlquist).

0301-4622/02/$ - see front matter
PII: S0301-4622(02)00157-6

a result of the motors switching to clockwise rotation [3]. In response to temporal changes in chemoattractant concentrations, the switching frequency of the flagellar motor is modulated such that *E. coli* decrease the frequency of tumbling when attractant concentrations increase over time, and increase the frequency of tumbling when concentrations decrease over time [4]. This simple behavior allows the bacteria to migrate up chemoattractant gradients and down chemorepellent gradients.

The chemotaxis system in bacteria is governed by a variety of transient protein–protein interactions. Complexes form and dissociate and information is passed from molecule to molecule through conformational change. While chemotaxis is one of the most comprehensively studied two-component bacterial signal-transduction pathways (for reviews see [5–7]) and the individual structures of the relevant molecules involved have been solved, fundamental questions still remain about the nature of the physical interactions of the molecules involved.

Dissociation of an attractant ligand from the periplasmic domain of the adapted receptor causes a conformational change in its transmembrane receptor [8]. This conformational change is transduced across the periplasmic membrane and is believed to cause a conformational change in the complex formed by CheA, CheW and the cytoplasmic domain of the receptor. The result of ligand dissociation is an increase in the autophosphorylation rate of CheA [9]; this has the direct consequence of increasing the ratio of phosphorylated/unphosphorylated CheY. Phospho-CheY modulates the switching frequency of the flagellar motor [10,11].

CheW is an essential protein component of the bacterial chemotaxis pathway [12]. The chemotaxis signaling complex contains CheW, one or another transmembrane receptor and the histidine auto-kinase CheA (for review see [13]). CheW appears to act as a coupling protein to allow enhanced affinity of the receptor and kinase. In the absence of CheW, ternary signaling complexes are either not formed or poorly formed [14]. In addition, these complexes assemble in a CheW-dependent manner into a supra-molecular complex with polar localization in vivo [15,16].

The work presented here describes the backbone dynamics of CheW from *Thermotoga maritima* as determined from ^{15}N spin relaxation NMR spectroscopy. Using the 'model-free' approach, order parameters, S^2, the $\{^1H\}-^{15}N$ heteronuclear NOE values and the chemical exchange rate, R_{ex}, show that the amide backbone of CheW exhibits considerable motional freedom from the picosecond to millisecond time scales. Combined with the three-dimensional structure of CheW from *T. maritima* (Fig. 1) [17] and two mutational studies put forward by Liu and Parkinson [18] and Boukhvalova et al. [19], analysis of ^{15}N relaxation data

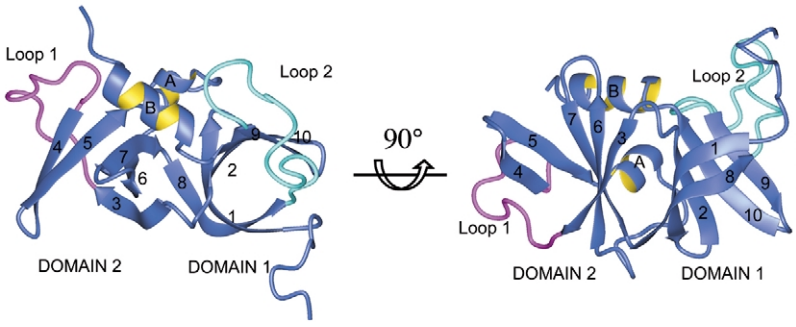

Fig. 1. Ribbon diagrams of CheW from *T. maritima.* Secondary structural elements are noted. Loop 1 is shown in cyan and loop 2 is shown in magenta for clarity. The structure consists of two five-stranded β strands joined by an extensive hydrophobic core. Domain 1 consists of strands 1, 2, 8, 9 and 10 shown at the right of the figure. Domain 2 is made of strands 3, 4, 5, 6 and 7, as well as helixes A and B, and is shown at the right of the structure. Loop 1 is located between strands 3 and 4, while loop 2 is between strands 8 and 9. Ribbon diagrams created with MOLMOL [39].

paint a valuable picture of the multifunctional surface of CheW.

2. Experimental

2.1. Sample preparation

CheW was expressed from the plasmid pCW/TMW in *E. coli* strain M15 pREP4 [20]. Isotopic labeling was achieved by expression of CheW at 37 °C in M9T minimal media. Media contained 1.0 g l^{-1} $^{15}NH_4Cl$ (Isotec Inc) as the sole nitrogen source for ^{15}N uniformly labeled protein samples. The bacteria were grown to an optical density of 0.5 at 600 nm before induction. Protein production was begun with the addition of 1 mM isopropyl β-D-thiogalactopyranoside (IPTG). CheW was purified as previously described [20]. Collected fractions were pooled and tested for purity by reverse-phase HPLC. The purified protein was then dialyzed against 2 l of final NMR buffer (50 mM sodium acetate, 25 mM sodium chloride, 0.02% sodium azide) for 24 h. Protein samples were concentrated to ~1 mM, as measured by bicinchoninic acid (BCA Pierce) assay with Centricon 10 concentrators (Amicon). NMR samples contained 50 mM sodium acetate, pH 4.5, 25 mM KCl, 0.02% sodium azide. 10% D_2O was added to lock the signal.

2.2. ^{15}N relaxation

Relaxation experiments were carried out on a single sample of uniformly ^{15}N labeled CheW at ~1.0 mM. NMR spectroscopy was carried out at 308 K on a Varian Inova 600-MHz spectrometer equipped with a $^1H[^{13}C/^{15}N]$ pulse-field gradient probe. The spectrometer was operated at a ^{15}N frequency of 60.8 MHz and a ^1H frequency of 599.9 MHz. Spectra were collected for measurement of the longitudinal relaxation rates (R_1), the ^{15}N transverse relaxation rates (R_2) and the $\{^1H\}$–^{15}N steady-state NOE of the ^{15}N nuclei in CheW [21]. The pulse sequences included sensitivity enhancement and gradient selection [22]. Spectra were recorded with 256×512 points and sweep widths of 2000×8000 Hz in the indirect nitrogen dimension and direct proton dimension, respectively. R_1 relaxation was determined from spectra recorded with delays of 218.0, 437.0, 655.0, 873.0, 1200, 1420 and 1640 ms with 32 scans per t_1 period. A recycle delay of 1.5 s was used. R_2 relaxation was determined from spectra recorded with CPMG times of 16.8, 33.6, 50.3, 67.1, 83.9, 100.7, 117.9 and 151.0 ms, with 32 scans per t_1 period. A recycle delay of 1.5 s was used. The steady-state NOE was measured by taking a pair of spectra with and without proton saturation. The ^1H saturation was achieved with 120 proton pulses applied every 5 ms. Data sets were identically processed using FELIX95 (Molecular Simulations Inc).

2.3. Data analysis

Peak heights were measured for each spectrum in the series at a fixed amide resonance position. The determination of R_1 and R_2 values for each amide was carried out by fitting the series of measured intensities to the equation:

$$I(t) = I_0 * \exp(-R_{1,2}t) + C \quad (1)$$

where $I(t)$ is the intensity at time t and I_0 is the intensity at time zero. Non-linear least-squares fitting as implemented by the KALEIDAGRAPH program (Synergy Software) was employed for the optimization of I_0 and $R_{1,2}$ values. The $\{^1H\}$–^{15}N steady-state values were determined from the ratio of the peak intensities with and without proton saturation ($I_{NOE}/I_{NO\text{-}NOE}$). The relaxation of the amide ^{15}N nuclear spin is dominated by the interaction of the dipole with the spin of the directly attached proton and by chemical shift anisotropy. The equations that describe this relaxation are [23]:

$$R_1 = (d^2/4)[J(\omega H - \omega N) + 3J(\omega N) + 6J(\omega H + \omega N)] + c^2 J(\omega N) \quad (2)$$

$$R_2 = (d^2/8)[4J(0) + [J(\omega H - \omega N) + 3J(\omega N) + 6J(\omega H) + 6J(\omega H + \omega N)] + (c^2/6)[4J(0) + 3J(\omega N)] + R_{ex} \quad (3)$$

$$NOE = 1 + (d^2/4R_1)(\gamma H/\gamma N)[6J(\omega H + \omega N) - J(\omega H - \omega N)] \quad (4)$$

where $d=(\mu^0 h\gamma N\gamma H/8\pi^2)\langle r_{NH}^{-3}\rangle$; $c=\omega N\Delta\sigma/\sqrt{3}$; μ^0 is the permeability in a vacuum; h is Planck's constant; γN and γH are the gyromagnetic ratios of ^{15}N and ^{1}H, respectively; r_{NH} is the interatomic distance of the proton–nitrogen bond; ωH and ωN are the Larmor frequencies of ^{15}N and ^{1}H, respectively; and $\Delta\sigma$ is the chemical shift anisotropy for ^{15}N nuclei. An R_{ex} term is included in Eq. (3) to account for chemical exchange processes that contribute to the decay of transverse magnetization during the experiment used to measure R_2. Using an extended version of the 'model-free' formalism of Lipari and Szabo [24–26], the amplitudes and time scales of the internal motions were determined from the relation data using the program MODELFREE [27]. This approach uses the spectral density function $J(\omega)$ modeled as [24]:

$$J(\omega)=2/5S_f^2\left\{\left[S_s^2\tau_m/(1+(\omega\tau_m)^2)\right]+\left[(1-S_s^2)\tau_e/(1+(\omega\tau_e)^2)\right]\right\} \quad (5)$$

where $\tau_e=\tau_s\tau_m/(\tau_s+\tau_m)$; τ_m is the overall rotational correlation time; τ_e is the effective internal correlation time; τ_f is the effective internal correlation time on a fast time scale, $\tau_e=\tau_f$, $\tau_f<100$–200 ps; τ_s is the effective internal correlation on a slow time scale, $\tau_e=\tau_s$, $\tau_f<\tau_s<\tau_m$; $S^2=S_s^2\ S_f^2$ is the square of the generalized order parameter and is representative of the degree of spatial restriction of the internal motion. S_f^2 and S_s^2 are the squares of the order parameters in the fast and slow time scales, respectively. The generalized order parameter reflects motions that are on the pico–nanosecond time scale, with $S^2=1$ completely restricted to 0 for completely isotropic motion.

Five models were tested for each ^{15}N spin for which relaxation parameters could be measured in CheW. The parameters describing the internal motion were calculated using the isotropic diffusion model using the program MODELFREE [27]. Model 1 calculates only S^2, making the assumption that internal motions are extremely fast (<20 ps) and that motions on the slow time scale are negligible, $S_s^2=1$ and $\tau_f\to 0$. Model 2 calculates S^2 and τ_f and assumes that $S_s^2=1$ and slow motions are negligible. Model 3 is derived from model 1, but includes an R_{ex} contribution to the relaxation to account for chemical exchange processes. Model 4 is a derivative of model 2, but includes a non-zero R_{ex} term. Model 5 assumes that there are fast and slow time-scale motions and calculates order parameters for both the fast (S_f^2) and slow (S_s^2) motions, as well as the correlation times for the internal motions, $\tau_e=\tau_s$ and assumes $\tau_f\to 0$. The initial estimate of the overall rotational correlation time, τ_m, was calculated from the ratio of R_1/R_2 trimmed to one standard deviation of the mean using the program TMEST [27,28]. Data were fitted to each of the five dynamic models, with τ_m fixed at the initial estimate. A single model was then chosen to describe the dynamic behavior of the ^{15}N spins by Monte Carlo simulations and application of the *F*-statistic test as described by Mandel et al. [29]. Once a model was chosen for each ^{15}N spin, the τ_m and the internal motion parameters were simultaneously optimized. Uncertainties in the parameters obtained were estimated by Monte Carlo sampling, as implemented in the program MODELFREE. In addition, an axial symmetric model based on the diffusion tensor calculated from the NMR solution structure of CheW was also tested. This model was found not to be statistically significant in describing the relaxation data.

3. Results

A single sample of uniformly ^{15}N labeled CheW was used for characterization of the relaxation properties of CheW. The ^{15}N longitudinal relaxation rate (R_1), the ^{15}N transverse relaxation rate (R_2) and the $\{^1H\}-^{15}N$ steady-state NOE values were determined at 60.8 MHz by the analysis of proton-detected $^1H-^{15}N$ heteronuclear correlation spectroscopy [28]. Relaxation parameters were measured for 134 of the 148 non-proline amides at 35 °C. Spectral overlap precluded the accurate measurement of residues 6, 18, 21, 27, 34, 66, 74, 80, 96, 99, 103 and 138. R_1 and R_2 values were calculated by linear least-squares fitting of a single exponential decay to the experimental data. The NOE value was calculated by taking the ratio of peak intensity with and without ^1H NOE enhancement. Fig. 2a–c show the values measured for the relaxation parameters for CheW vs. residue number. Tabulated data for R_1, R_2 and the $\{^1H\}-^{15}N$

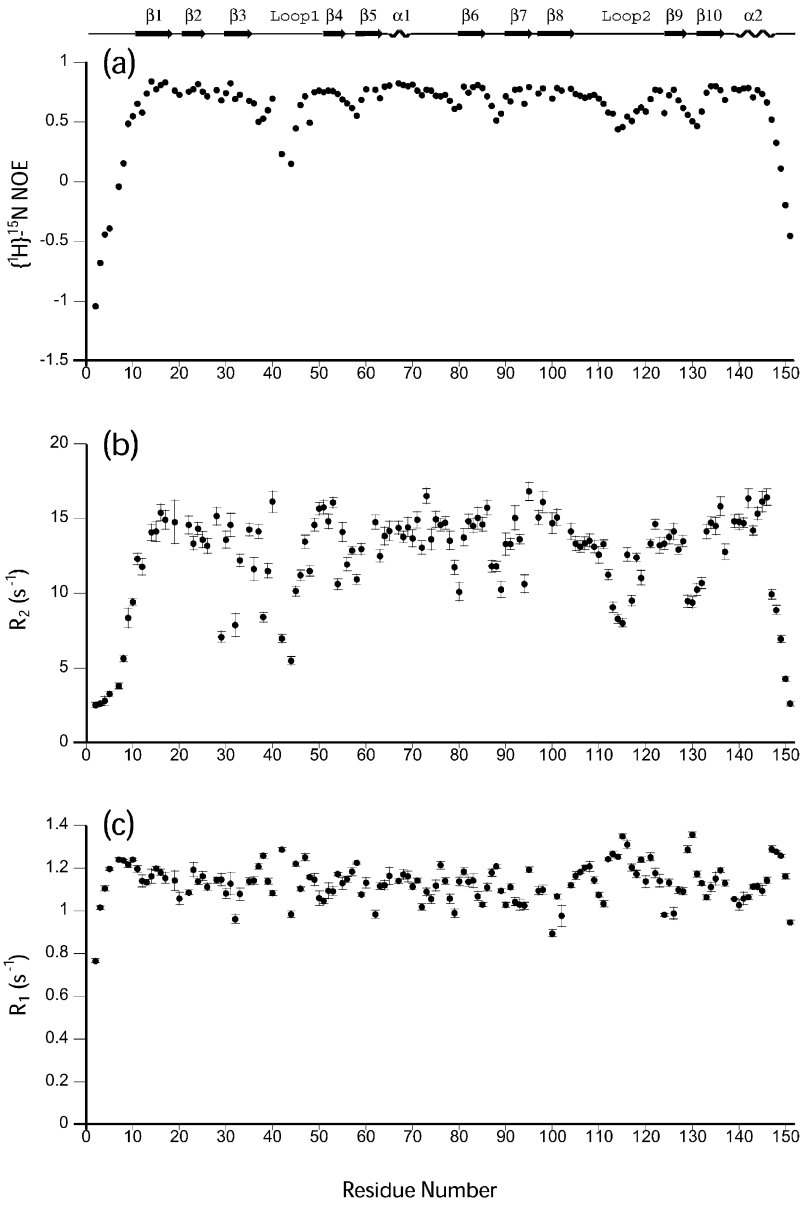

Fig. 2. Backbone ^{15}N relaxation parameters at 600 MHz for CheW vs. residue number. Approximate location of secondary structural elements is shown at the top: (a) $\{^1H\}-^{15}N$ NOE; (b) ^{15}N R_2; and (c) ^{15}N R_1. Data were unavailable for the three proline residues at positions 41, 43 and 61, as well as for the N-terminal methionine. Spectral overlap precluded the measurement of residues 6, 18, 21, 27, 34, 66, 96, 80, 99, 103 and 138.

steady-state NOE are given in Table 1. The mean values for R_1, R_2 and $\{^1H\}-^{15}N$ steady-state NOE were 1.13, 12.8 and 0.61 respectively. To extract the parameters describing the internal motion, we analyzed the R_1, R_2 and, $\{^1H\}-^{15}N$ NOE data gathered on CheW using the extended 'model-free' approach of Lapari and Szabo as implemented in the MODELFREE program using an isotropic

model to describe the diffusion [24–26]. This approach provides information on the internal and overall motions of the molecule of interest. The ^{15}N R_1, R_2 and $\{^1H\}-^{15}N$ NOE data were fitted to five dynamic models, with τ_m fixed at 10.441 ns, assuming an isotropic rotational diffusion model. Based on the criteria outlined by Mandel et al., a single model was chosen to represent each ^{15}N spin [29]. The number of residues represented by each of the five models was 23, 16, 20, 33 and 42 for models 1–5, respectively. The residues fit by model 1 were 14, 15, 19, 23, 25, 30, 31, 49, 64, 65, 68–70, 81, 83, 122, 123, 125, 135 and 139–142. The residues fit by model 2 were 12, 26, 33, 36, 39, 57, 63, 79, 94, 105–110 and 127. The residues fit by model 3 were 16, 17, 24, 28, 50, 60, 62, 67, 73, 84, 85, 93, 95, 98, 101, 104, 126, 134, 137 and 144. The residues fit by model 4 were 13, 20, 21, 35, 37, 40, 51–53, 55, 59, 71, 72, 75–78, 82, 86, 90–92, 97, 100, 111, 120, 124, 128, 133, 136, 143, 145 and 146. The residues fit by model 5 were 2–11, 29, 32, 38, 42, 44–48, 54, 56, 58, 87–89, 112–119, 121, 129–132 and 147–151. All of the ^{15}N spins for which data were available could be represented by one of the five models. The parameters representing the internal motion, as well as τ_m, were simultaneously fitted to the experimental data using the dynamic model chosen for each amide ^{15}N spin. The final τ_m was determined to be 10.588 ns, as compared to the initial estimate of 10.411 ns. Fig. 3a–c show the extracted parameters describing the internal motion of CheW vs. residue number. Values for S^2, τ_e and R_{ex}, as well as the model used for each spin, are given in Table 2.

3.1. Picosecond–nanosecond motions

Small or negative NOE values represent the presence of motion on the picosecond–nanosecond time scale. The only NOE values in CheW that were negative were residues 2–5 in the N-terminus and residues 150 and 151 in the C-terminus (see Fig. 2a). The finding that the termini exhibit significant flexibility was not surprising, given that these residues appear disordered in the structural ensemble [17]. As shown in Fig. 4, the NOE values observed mirror the calculated RMSD quite

Table 1
Relaxation parameters of CheW at 35 °C

Residue number	R_1 (s^{-1})	R_2 (s^{-1})	NOE
2	0.767	2.546	−1.041
3	1.016	2.627	−0.675
4	1.105	2.821	−0.440
5	1.198	3.272	−0.391
6			
7	1.240	3.825	−0.038
8	1.237	5.642	0.155
9	1.216	8.365	0.488
10	1.241	9.419	0.547
11	1.197	12.300	0.654
12	1.141	11.777	0.578
13	1.134	18.511	0.737
14	1.163	14.068	0.840
15	1.200	14.154	0.775
16	1.181	15.397	0.809
17	1.154	14.926	0.833
18			
19	1.142	14.780	0.761
20	1.059	25.487	0.726
21			
22	1.087	14.569	0.754
23	1.192	13.349	0.775
24	1.137	14.340	0.816
25	1.163	13.586	0.753
26	1.113	13.175	0.716
27			
28	1.144	15.161	0.768
29	1.146	7.090	0.682
30	1.082	13.591	0.743
31	1.128	14.567	0.826
32	0.962	7.875	0.693
33	1.079	12.210	0.727
34			
35	1.138	14.254	0.675
36	1.143	11.638	0.658
37	1.209	14.148	0.503
38	1.257	8.408	0.528
39	1.139	11.506	0.600
40	1.083	16.135	0.698
41			
42	1.287	6.983	0.234
43			
44	0.983	5.494	0.151
45	1.220	10.149	0.447
46	1.103	11.211	0.643
47	1.252	13.455	0.716
48	1.158	11.506	0.492
49	1.147	14.573	0.750
50	1.060	15.658	0.763
51	1.048	15.777	0.750
52	1.095	14.822	0.762
53	1.094	16.069	0.757
54	1.173	10.618	0.734

Table 1 *(Continued)*

Residue number	R_1 (s^{-1})	R_2 (s^{-1})	NOE
55	1.129	14.102	0.690
56	1.149	11.943	0.657
57	1.183	12.882	0.617
58	1.225	10.936	0.551
59	1.078	12.976	0.686
60	1.132	19.902	0.773
62	0.983	14.769	0.771
61			
63	1.117	12.496	0.700
64	1.121	13.836	0.798
65	1.164	14.179	0.806
66			
67	1.141	14.397	0.826
68	1.172	13.787	0.807
69	1.162	14.437	0.803
70	1.115	13.670	0.813
71	1.144	14.910	0.762
72	1.019	13.070	0.725
73	1.090	16.514	0.771
74	1.056	13.604	0.763
75	1.119	14.957	0.719
76	1.214	14.579	0.717
77	1.140	14.723	0.726
78	1.057	13.539	0.676
79	0.989	11.747	0.610
80	1.137	10.112	0.627
81	1.185	13.749	0.798
82	1.136	14.815	0.747
83	1.142	14.522	0.795
84	1.069	15.032	0.809
85	1.030	14.620	0.786
86	1.111	15.743	0.715
87	1.179	11.817	0.634
88	1.208	11.816	0.514
89	1.096	10.245	0.574
90	1.028	13.298	0.716
91	1.113	13.305	0.672
92	1.043	15.046	0.771
93	1.030	13.618	0.772
94	1.025	10.643	0.652
95	1.192	16.809	0.792
96			
97	1.095	15.072	0.739
98	1.099	16.113	0.783
99			
100	0.895	14.694	0.698
101	1.068	15.093	0.785
102	0.978	27.559	0.761
103			
104	1.121	14.149	0.778
105	1.166	13.334	0.733
106	1.181	13.134	0.719
107	1.203	13.357	0.703
108	1.208	13.525	0.717

Table 1 *(Continued)*

Residue number	R_1 (s^{-1})	R_2 (s^{-1})	NOE
109	1.144	13.128	0.728
110	1.075	12.579	0.697
111	1.034	13.292	0.652
112	1.243	11.242	0.581
113	1.266	9.079	0.572
114	1.254	8.308	0.441
115	1.351	8.030	0.460
116	1.312	12.606	0.544
117	1.203	9.518	0.511
118	1.174	12.414	0.591
119	1.241	11.047	0.621
120	1.138	21.927	0.586
121	1.252	13.336	0.692
122	1.178	14.630	0.770
123	1.141	13.208	0.763
124	0.981	13.334	0.574
125	1.132	13.777	0.722
126	0.989	14.146	0.770
127	1.099	12.920	0.682
128	1.092	13.501	0.617
129	1.287	9.478	0.561
130	1.357	9.399	0.506
131	1.173	10.256	0.466
132	1.129	10.686	0.587
133	1.064	14.138	0.749
134	1.112	14.729	0.801
135	1.152	14.516	0.803
136	1.192	15.824	0.768
137	1.129	12.769	0.685
138			
139	1.055	14.821	0.777
140	1.028	14.783	0.766
141	1.059	14.719	0.782
142	1.064	16.355	0.787
143	1.115	14.204	0.707
144	1.114	15.336	0.765
145	1.095	16.136	0.734
146	1.143	16.429	0.664
147	1.288	9.938	0.522
148	1.277	8.893	0.327
149	1.258	6.952	0.113
150	1.162	4.274	−0.194
151	0.947	2.618	−0.452

well. When the NOE values are mapped to the structure of CheW, regions of CheW that show low NOE values correspond to loop 1, the hairpin at the end of strands 4/5, the end of the hairpin composed of strands 6/7, loop 2 and the end of the hairpin of strands 9/10 (Fig. 5a). These regions of low NOE values closely match regions

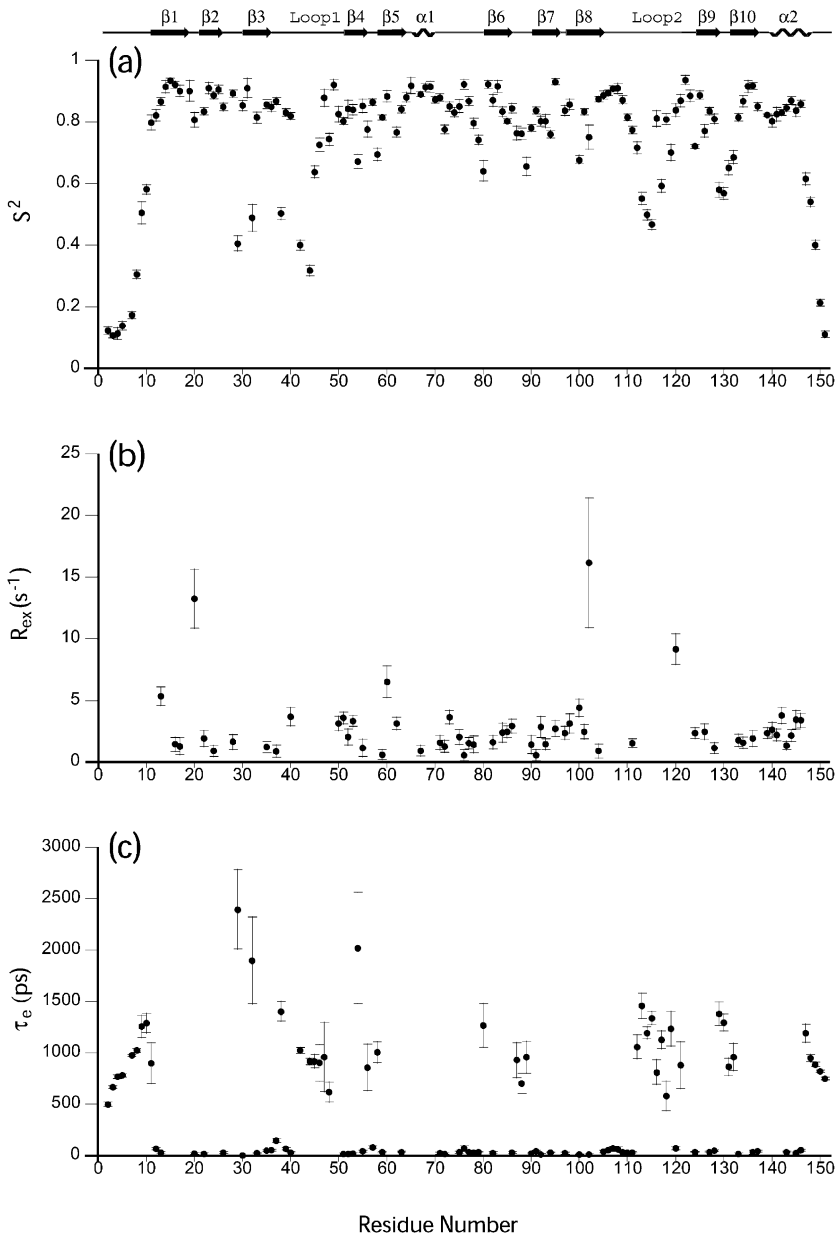

Fig. 3. Backbone ^{15}N parameters describing the internal motion of CheW at 600 MHz vs. residue number. Approximate location of secondary structural elements is shown at the top: (a) S^2; (b) R_{ex}; and (c) τ_e.

of the protein that had high root mean square deviation (RMSD) in position within the structural ensemble (Fig. 5b). Loops 1 and 2 appeared disordered in the structural ensemble and their low NOE values confirmed that this disorder was due to fast time scale motion rather than an under-determination of the structure in this region. In CheA, however, each of these loops participates in a protein–protein interaction either via crystal or inter-domain contact [30]. The ends of the

hairpins formed by strands 4/5 and 6/7 together form the top of the β-barrel formed by domain 2 of CheW, and show a slight increase in backbone RMSD over residues closer to the central hydrophobic core. This result is consistent with the limited number of long-range NOEs observed in the structure solution and indicates that the residues may also fluctuate on a fast time scale.

Fast (pico–nanosecond) motions of the amide HN bond vector are expressed in terms of the square of the order parameter (S^2), ranging from 0 (unrestricted motion) to 1 (completely restricted motion). Generally, rigid regions of the protein have S^2 values of approximately 8.5 or greater, while flexible regions of the protein have S^2 values below 8.0. The order parameter S^2 obtained from the isotropic model showed a significant spread in values throughout the CheW protein chain (Fig. 3a). The N and C termini had S^2 values as low as 0.11. Of the 134 ^{15}N spins for which data were available, 52 had S^2 values below 0.8. This, combined with low overall NOE values, indicates that CheW is highly mobile on the picosecond–nanosecond time scale with respect to the overall tumbling of the molecule. Other regions that showed low S^2 values were loops 1 and 2, as well as the end of the hairpin formed by strands 9 and 10 (Fig. 6). The residues that have S^2 values above 8.5 are 13–17, 23–26, 28, 30, 31, 33, 35–37, 49, 55, 57, 60, 63–65, 67–71, 73, 75–77, 81–83, 95, 97–98 104–109, 121, 123, 125, 134–137 and 143–146. These residues cluster around the central hydrophobic core of CheW and indicate that this probably forms the rigid framework of CheW.

3.2. Microsecond–millisecond motions

Amide bonds that undergo chemical or conformational exchange on the slow (micro–millisecond) time scale are manifest by non-zero R_{ex} values. Model-free analysis indicates that there are several regions of CheW that experience fluctuations in this time regime (Fig. 3c). The residues that exhibited R_{ex} values greater than 1 s^{-1} were 13, 16, 17, 20, 22, 28, 35, 37, 40, 50–53, 55, 60, 62, 71–73, 75, 77, 78, 82, 84–86, 90, 92, 93, 95, 97, 98, 100–102, 111, 120, 124, 126, 128, 133,

Table 2
Parameters describing the internal motions of CheW at 35 °C

Residue number	S^2	R_{ex} (Hz)	τ_e (ms)	Model number
2	0.124		498.65	5
3	0.108		665.39	5
4	0.114		767.82	5
5	0.139		780.12	5
6				
7	0.173		976.84	5
8	0.306		1025	5
9	0.505		1258.4	5
10	0.581		1290.9	5
11	0.798		899.42	5
12	0.821		67.789	2
13	0.866	5.36	30.526	4
14	0.914			1
15	0.935			1
16	0.92	1.445		3
17	0.9	1.283		3
18				
19	0.901			1
20	0.807	13.236	22.063	4
21				
22	0.834	1.917	18.87	4
23	0.91			1
24	0.887	0.898		3
25	0.905			1
26	0.849		31.79	2
27				
28	0.892	1.642		3
29	0.406		2394.2	5
30	0.853			1
31	0.91			1
32	0.489		1899.8	5
33	0.814		23.923	2
34				
35	0.857	1.23	49.705	4
36	0.849		54.893	2
37	0.868	0.896	149.23	4
38	0.503		1404	5
39	0.831		67.871	2
40	0.82	3.675	31.454	4
41				
42	0.4		1024.1	5
43				
44	0.318		915.79	5
45	0.638		916.58	5
46	0.726		904.01	5
47	0.878		958.81	5
48	0.744		618.51	5
49	0.921			1
50	0.826	3.134		3
51	0.803	3.59	16.266	4
52	0.842	2.05	17.72	4
53	0.839	3.328	18.995	4
54	0.672		2017.6	5

Table 2 *(Continued)*

Residue number	S^2	R_{ex} (Hz)	τ_e (ms)	Model number
55	0.852	1.148	42.917	4
56	0.776		857.9	5
57	0.864		82.15	2
58	0.695		1006.5	5
59	0.814	0.607	33.037	4
60	0.883	6.522		3
62	0.767	3.148		3
61				
63	0.841		37.527	2
64	0.88			1
65	0.918			1
66				
67	0.89	0.914		3
68	0.912			1
69	0.914			1
70	0.872			1
71	0.879	1.576	24.354	4
72	0.776	1.285	18.477	4
73	0.85	3.637		3
74	0.831			1
75	0.851	2.03	32.716	4
76	0.922	0.569	72.722	4
77	0.868	1.533	35.474	4
78	0.796	1.437	31.837	4
79	0.742		33.445	2
80	0.641		1268.7	5
81	0.922			1
82	0.87	1.606	27.785	4
83	0.915			1
84	0.833	2.4		3
85	0.803	2.452		3
86	0.844	2.919	32.182	4
87	0.764		929.27	5
88	0.762		702.21	5
89	0.656		956.97	5
90	0.781	1.426	20.963	4
91	0.837	0.577	43.386	4
92	0.803	2.858	11.647	4
93	0.803	1.445		3
94	0.76		31.31	2
95	0.93	2.719		3
96				
97	0.837	2.362	23.66	4
98	0.857	3.125		3
99				
100	0.677	4.401	14.373	4
101	0.833	2.472		3
102	0.751	16.162	10.232	4
103				
104	0.874	0.897		3
105	0.887		40.239	2
106	0.894		54.866	2
107	0.908		73.935	2
108	0.909		63.304	2

Table 2 *(Continued)*

Residue number	S^2	R_{ex} (Hz)	τ_e (ms)	Model number
109	0.871		36.188	2
110	0.815		30.03	2
111	0.774	1.522	32.481	4
112	0.716		1058.2	5
113	0.552		1459.8	5
114	0.498		1193.4	5
115	0.467		1338.4	5
116	0.811		810.36	5
117	0.592		1128.2	5
118	0.809		583.54	5
119	0.701		1236.6	5
120	0.838	9.168	72.003	4
121	0.869		881.56	5
122	0.936			1
123	0.885			1
124	0.721	2.354	36.363	4
125	0.887			1
126	0.771	2.458		3
127	0.835		37.675	2
128	0.81	1.163	50.07	4
129	0.58		1381.4	5
130	0.568		1296.8	5
131	0.651		865.8	5
132	0.686		960.93	5
133	0.815	1.771	17.829	4
134	0.867	1.584		3
135	0.915			1
136	0.917	1.91	33.712	4
137	0.85		44.434	3
138				
139	0.822	2.355		3
140	0.802	2.631		3
141	0.825	2.207		3
142	0.83	3.781		3
143	0.845	1.362	35.121	4
144	0.869	2.165		3
145	0.836	3.444	24.865	4
146	0.858	3.384	54.325	4
147	0.615		1193.4	5
148	0.541		950.89	5
149	0.401		885.97	5
150	0.214		821.59	5
151	0.112		748.07	5

134, 136 and 139–146. When mapped into the structure of CheW, these residues cluster primarily to the β hairpins formed by strands 4/5, stand 6/7 and helix B (Fig. 7a). The implication of non-zero R_{ex} terms is that these structural elements undergo fluctuation between at least two states. This result, combined with the S^2 and NOE results,

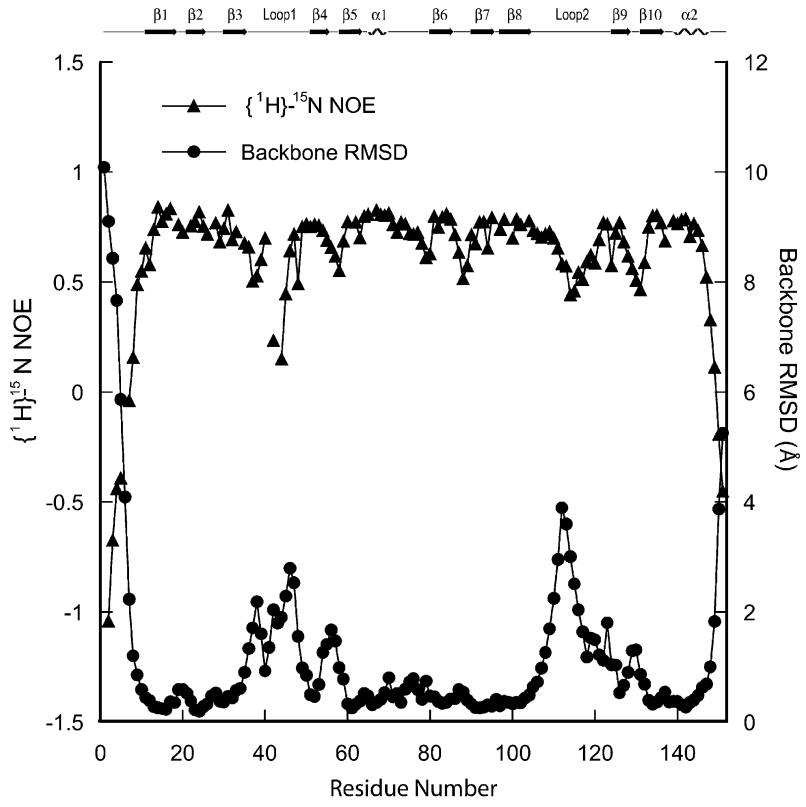

Fig. 4. $\{^1H\}-^{15}N$ NOE and backbone RMSD vs. residue number. Left scale for $[^1H]-^{15}N$ NOE in blue and right scale for RMSD in red.

indicates that the 4/5, 6/7 hairpins and helix B likely experience motions on both the milli–microsecond and pico–nanosecond time scales.

4. Discussion

It is becoming increasingly clear that NMR-derived dynamics information can provide clues about the interaction surfaces in proteins. In some cases, unfolded regions in individual proteins are observed that become structured upon interaction with other macromolecular components [31,32], while in others the presence of millisecond dynamics in certain regions indicates regions coupled to binding and other functional events [33–35].

Analysis of the ^{15}N relaxation parameters for CheW has revealed that CheW exhibits a high degree of motion on the pico–microsecond time scale. The results from this study show that loops 1 and 2, which show a high degree of variability in the structural ensemble solved, have dynamic fluctuations on the pico–nanosecond time scale, but not in the milli–microsecond regime. This result implies that loops 1 and 2 have extreme conformational freedom, usually associated with the termini of a protein chain.

A somewhat unexpected outcome of this analysis was that the top of domain 2 experienced relaxation on the milli–microsecond time scale, as measured by R_{ex} (Fig. 7a). In the structural ensemble these regions were ordered as measured by backbone RMSD. These regions of high R_{ex} co-localize will the regions of CheW affected by CheA binding, and thus this conformational exchange may indicate partitioning between states, one of which is competent to bind CheA in the receptor complex. This is analogous to what has

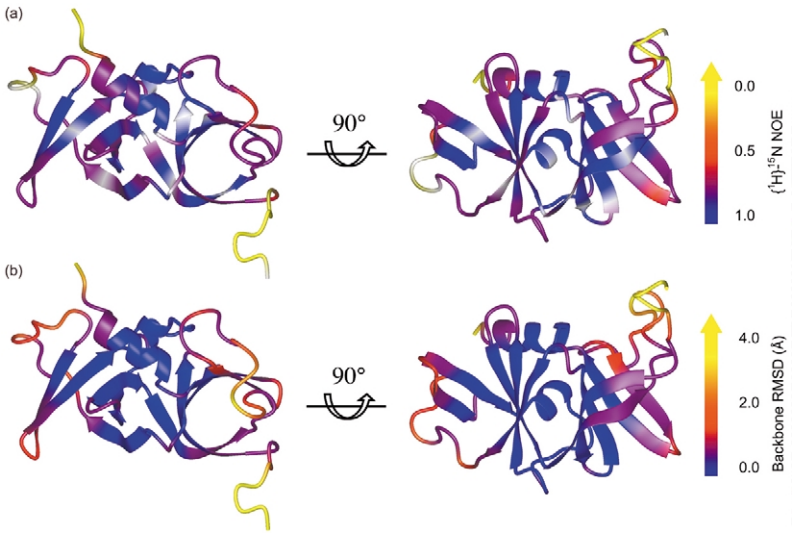

Fig. 5. Ribbon diagram representations of CheW, colored based on the $\{^1H\}$-^{15}N NOE and the backbone RMSD. (a) Ribbon diagram of CheW representing $\{^1H\}$-^{15}N NOE values as a continuous color scale, as indicated. (b) Ribbon diagram of CheW representing the RMSD on a continuous color scale, as indicated.

been found in the response regulator NTRC. Volkman and co-workers [36,37] were able to show through dynamics experiments that NTRC was partitioning between states and that phosphorylation of this molecule only served to shift the population distribution of these states. In this system, high R_{ex} values also co-localize with the mutations thought to effect receptor binding, again highlighting a possible binding interface [18] (Fig. 7b, green spheres).

When the crystal structure of CheA was solved in the Simon laboratory, they recognized that the regulatory domain of CheA is similar in amino acid sequence to CheW and suggested that the two proteins share a common fold. Our solution structure of CheW confirmed this homology. In CheA, the regions homologous to loops 1 and 2 of CheW are ordered, loop 1 forming β strands and loop 2 forming a loose helix [30]. In CheA, however, these loops participate in protein–protein interactions either via crystal or interdomain contact. The region corresponding to loop 1 participates in a crystal contact with a symmetry-related molecule, while the region corresponding to loop 2 packs

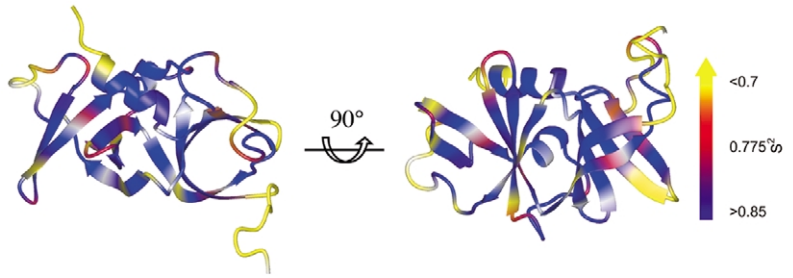

Fig. 6. Ribbon diagram representations of CheW colored based on the S^2 value represented with a continuous color scale, as indicated.

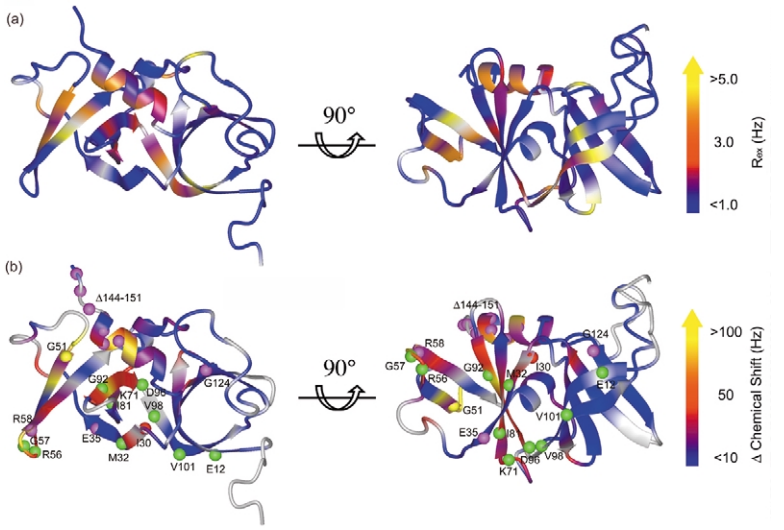

Fig. 7. Ribbon diagram representations of CheW showing R_{ex} values and chemical shift changes associated with CheA binding superimposed with mutational data. (a) Ribbon diagram representation of CheW, colored based on the R_{ex} value represented with a continuous color scale, as indicated. (b) Ribbon diagram of CheW with a continuous color ramp showing chemical shift changes upon CheA binding. Sites of suppressor mutations of receptor mutants depicted as green spheres [18]. Mutations effecting ternary complex formation depicted as purple spheres [19]. Mutations abolishing CheW binding to CheA and the receptor depicted as yellow and red spheres, respectively [19].

against the kinase domain of CheA. The implication is that these conserved loops may participate in mediating CheW interactions within the sensor kinase complex, with the loops only becoming ordered upon binding. Interestingly these two loops are immediately followed by two conserved glycines (Fig. 7b), the mutation of which eliminates CheA binding in the case of glycine 51 and ternary complex formation in the case of glycine 124 [19]. The dynamics results, together with the mutational data, further argue that these loops participate in protein–protein interactions in the receptor complex, likely becoming ordered upon complex formation. The chemical shifts of residues near loop 1 are affected by CheA binding, so it is not surprising that mutations in this region may effect CheA binding. Loop 2, however, is unaffected by CheA binding and seems removed from the mutations directly effecting receptor binding. The approximate two-fold symmetry of the CheW structure naturally suggests two surfaces for interaction with other protein components. This was likely part of the motivation of Shimizu et al. [38] to suggest that one domain interacts with CheA and the other with the receptor. With the exception of glycine 124, mutations affecting the formation of the ternary complex were found to localize to domain 1 [19] (Fig. 7b, purple spheres). The combination of chemical shift perturbation and genetic data argues that domain 2 (and loop 1) interacts with both CheA and the receptor. What then is the role of loop 2? It is unlikely that loop 2 as always unstructured in the cell. It is difficult to imagine a function that would require an unfolded chain. Furthermore, while the degree of amino acid identity is low for all CheW proteins in the sequence database, the extent of conservative amino acid substitution is very high in the CheW family. This holds true for the residues in loop 2. This again suggests that loop 2 is designed to interact with some other components and is likely to become structured upon such interaction, exploiting these conserved chemical properties. We

propose that loop 2 plays a role in forming the higher-order complexes observed at the cell poles.

Acknowledgments

This work was supported by a grant from the National Institutes of Heath (number GM57766).

References

[1] J.S. Parkinson, Signal transduction schemes of bacteria, Cell 73 (1993) 857–871.
[2] J.L. Appleby, J.S. Parkinson, R.B. Bourret, Signal transduction via the multi-step phosphorelay: not necessarily a road less traveled, Cell 86 (1996) 845–848.
[3] H.C. Berg, D.A. Brown, Chemotaxis in *Escherichia coli* analysed by three-dimensional tracking, Nature 239 (1972) 500–504.
[4] R.M. Macnab, D.E. Koshland, The gradient-sensing mechanism in bacterial chemotaxis, Proc. Natl. Acad. Sci. USA 69 (1972) 2509–2512.
[5] J.J. Falke, R.B. Bass, S.L. Butler, S.A. Chervitz, M.A. Danielson, The two-component signaling pathway of bacterial chemotaxis: a molecular view of signal transduction by receptors, kinases, and adaptation enzymes, Annu. Rev. Cell Dev. Biol. 13 (1997) 457–512.
[6] J.A. Hoch, Two-component and phosphorelay signal transduction, Curr. Opin. Microbiol. 3 (2000) 165–170.
[7] A.M. Stock, V.L. Robinson, P.N. Goudreau, Two-component signal transduction, Annu. Rev. Biochem 69 (2000) 183–215.
[8] M.V. Milburn, G.G. Prive, D.L. Milligan, et al., Three-dimensional structures of the ligand-binding domain of the bacterial aspartate receptor with and without a ligand, Science 254 (1991) 1342–1347.
[9] D.F. McNally, P. Matsumura, Bacterial chemotaxis signaling complexes: formation of a CheA/CheW complex enhances autophosphorylation and affinity for CheY, Proc. Natl. Acad. Sci. USA 88 (1991) 6269–6273.
[10] M. Eisenbach, S.R. Caplan, Bacterial chemotaxis: unsolved mystery of the flagellar switch, Curr. Biol. 8 (1998) 444–446.
[11] M. Eisenbach, Control of bacterial chemotaxis, Mol. Microbiol. 20 (1996) 903–910.
[12] M.P. Conley, A.J. Wolfe, D.F. Blair, H.C. Berg, Both CheA and CheW are required for reconstitution of chemotactic signaling in *Escherichia coli*, J. Bacteriol. 171 (1989) 5190–5193.
[13] A. Bren, M. Eisenbach, How signals are heard during bacterial chemotaxis: protein–protein interactions in sensory signal propagation, J. Bacteriol. 182 (2000) 6865–6873.
[14] J.A. Gegner, D.R. Graham, A.F. Roth, F.W. Dahlquist, Assembly of an MCP receptor, CheW, and kinase CheA complex in the bacterial chemotaxis signal transduction pathway, Cell 70 (1992) 975–982.
[15] Y. Liu, M. Levit, R. Lurz, M.G. Surette, J.B. Stock, Receptor-mediated protein kinase activation and the mechanism of transmembrane signaling in bacterial chemotaxis, EMBO J. 16 (1997) 7231–7240.
[16] J.R. Maddock, L. Shapiro, Polar location of the chemoreceptor complex in the *Escherichia coli* cell, Science 259 (1993) 1717–1723.
[17] I.J. Griswold, H. Zhou, M. Matison, et al., The solution structure and interactions of CheW from *Thermotoga maritima*, Nat. Struct. Biol. 9 (2002) 121–125.
[18] J.D. Liu, J.S. Parkinson, Genetic evidence for interaction between the CheW and Tsr proteins during chemoreceptor signaling by *Escherichia coli*, J. Bacteriol. 173 (1991) 4941–4951.
[19] M. Boukhvalova, F.W. Dahlquist, R.C. Stewart, CheW binding interactions with CheA and Tar: importance for chemotaxis signaling in *Esherichia coli*, J. Biol. Chem. 277 (2002) 22251–22259.
[20] R.V. Swanson, M.G. Sanna, M.I. Simon, Thermostable chemotaxis proteins from the hyperthermophilic bacterium *Thermotoga maritima*, J. Bacteriol. 178 (1996) 484–489.
[21] N.A. Farrow, R. Muhandiram, A.U. Singer, et al., Backbone dynamics of a free and phosphopeptide-complexed Src homology 2 domain studied by ^{15}N NMR relaxation, Biochemistry 33 (1994) 5984–6003.
[22] S. Gzresiek, A. Bax, The importance of not saturating H_2O in protein NMR. Application to sensitivity enhancement and NOE measurements, J. Am. Chem. Soc. 115 (1993) 12593–12594.
[23] A. Abragam, Principles of Nuclear Magnetism, Clarendon Press, Oxford, 1961.
[24] G.M. Clore, A. Szabo, A. Bax, L.E. Key, P.C. Driscoll, A.M. Gronenborn, Deviations from the simple two-parameter model-free approach to the interpretation of nitrogen-15 nuclear magnetic relaxation of proteins, J. Am. Chem. Soc. 112 (1990) 4989–4991.
[25] G. Lipari, A. Szabo, Model-free approach to the interpretation of nuclear magnetic resonance relaxation in macromolecules. 1. Theory and range of validity, J. Am. Chem. Soc. 104 (1982) 4546–4559.
[26] G. Lipari, A. Szabo, Model-free approach to the interpretation of nuclear magnetic resonance relaxation in macromolecules. 2. Analysis of experimental results, J. Am. Chem. Soc. 104 (1982) 4559–4570.
[27] A.I. Palmer, M. Rance, P. Wright, Intramolecular motions of a zinc finger DNA-binding domain Xfin characterized by proton-detected natural-abundance ^{13}C heteronuclear NMR spectroscopy, J. Am. Chem. Soc. 113 (1991) 4371–4380.
[28] L.E. Kay, D.A. Torchia, A. Bax, Backbone dynamics of proteins as studied by ^{15}N inverse-detected heteronuclear NMR spectroscopy: application to staphylococcal nuclease, Biochemistry 28 (1989) 8972–8979.

[29] A.M. Mandel, M. Akke, A.G. Palmer, Backbone dynamics of *Escherichia coli* ribonuclease HI: correlations with structure and function in an active enzyme, J. Mol. Biol. 246 (1995) 144–163.
[30] A.M. Bilwes, L.A. Alex, B.R. Crane, M.I. Simon, Structure of CheA, a signal-transducing histidine kinase, Cell 96 (1999) 131–141.
[31] C.L. Phillips, M.R. Stark, A.D. Johnson, F.W. Dahlquist, Heterodimerization of the yeast homeodomain transcriptional regulators alpha 2 and a1 induces an interfacial helix in alpha 2, Biochemistry 33 (1994) 9294–9302.
[32] H.J. Dyson, P.E. Wright, Coupling of folding and binding for unstructured proteins, Curr. Opin. Struct. Biol. 12 (2002) 54–60.
[33] F.A. Mulder, A. Mittermaier, B. Hon, F.W. Dahlquist, L.E. Kay, Studying excited states of proteins by NMR spectroscopy, Nat. Struct. Biol. 8 (2001) 932–935.
[34] V.A. Feher, J. Cavanagh, Millisecond-time scale motions contribute to the function of the bacterial response regulator protein Spo0F, Nature 400 (1999) 289–293.
[35] E.Z. Eisenmesser, D.A. Bosco, M. Akke, D. Kern, Enzyme dynamics during catalysis, Science 295 (2002) 1520–1523.
[36] D. Kern, B.F. Volkman, P. Luginbuhl, M.J. Nohaile, S. Kustu, D.E. Wemmer, Structure of a transiently phosphorylated switch in bacterial signal transduction, Nature 402 (1999) 894–898.
[37] B.F. Volkman, D. Lipson, D.E. Wemmer, D. Kern, Two-state allosteric behavior in a single-domain signaling protein, Science 291 (2001) 2429–2433.
[38] T.S. Shimizu, N. Le Novere, M.D. Levin, A.J. Beavil, B.J. Sutton, D. Bray, Molecular model of a lattice of signaling proteins involved in bacterial chemotaxis, Nat. Cell Biol. 2 (2000) 792–796.
[39] R. Koradi, M. Billeter, K. Wuthrich, MOLMOL: a program for display and analysis of macromolecular structures, J. Mol. Graph. 14 (1996) 29–32, Also pp. 51–55.